THE JOURNAL OF PHYSICAL CHEMISTRY C

C: Surfaces, Interfaces, Porous Materials, and Catalysis

Micropore Filling and Multilayer Formation in Stöber Spheres upon Water Adsorption

Francisco Gallego-Gomez, Judit Farrando-Pérez, Cefe Lopez, and Joaquin Silvestre-Albero

J. Phys. Chem. C, **Just Accepted Manuscript** • DOI: 10.1021/acs.jpcc.0c05313 • Publication Date (Web): 01 Sep 2020

Micropore Filling and Multilayer Formation in Stöber Spheres Upon Water Adsorption

Francisco Gallego-Gómez, [ϕ,*] *Judit Farrando-Pérez,* [δ] *Cefe López,* [ϕ] *Joaquín Silvestre-Albero*[δ,*]

[ϕ]Instituto de Ciencia de Materiales de Madrid (ICMM), Consejo Superior de Investigaciones Científicas (CSIC), Spain

[δ]Laboratorio de Materiales Avanzados (LMA), Departamento de Química Inorgánica-IUMA, Universidad de Alicante, Spain

* francisco.gallego@icmm.csic.es

* joaquin.silvestre@ua.es

ABSTRACT

The presence of porosity critically affects the performance of solid systems. The pore accessibility to adsorbate molecules and the corresponding adsorption/desorption behavior are crucial aspects to understand the properties of porous materials, but are difficult to address, principally when dealing with narrow micropores. A prominent example is colloidal silica (Stöber) spheres, whose microporosity, inaccessible for some adsorbates, can be readily filled by water molecules to a large extent, but exhibiting a complex adsorption behavior with unexpected hystereses. Here we perform water adsorption isotherms on Stöber spheres at different temperatures, using an original analysis of the Dubinin-Radushkevich representation to examine both the accessibility to the microporosity and the formation of water multilayers on the outer spheres surface. The micropore filling (and emptying) is found to be limited by the kinetic energy of the water molecules, causing low-pressure hysteresis. We further discover that the (temperature-dependent) completion of the micropore filling delays the onset of multilayer adsorption, leading to hysteresis at high relative pressure. The number of adsorbed water layers is determined, and the adsorption-induced swelling of the spheres is discussed.

INTRODUCTION

The adsorption properties of porous systems obviously depend on the amount and size of the porosity and the affinity between adsorbent (pore walls) and adsorbate. However, kinetic aspects are often less considered, although they decisively determine the accessibility of the adsorbed molecules to the inner space of porous material, which additionally may affect the adsorption on outer surfaces. However, the study of such features is challenging to-date –in particular, when microporosity (pore size of < 2 nm) is present– and new insights are necessary. The identification of kinetic restrains is of paramount importance to understand the equilibrium adsorption behavior in porous systems. In principle, kinetic restrictions can be unmasked by selecting probe molecules with different size/shape, or modifying the equilibrium criteria, although it is not an easy procedure.[1] Recently, we have investigated Stöber silica spheres by a combination of gas adsorption isotherms to evidence the distinct pore accessibility for different probe molecules.[2] It was directly demonstrated that N_2 (at –196 ºC) was unable to access the intricate inner porosity of Stöber spheres –a fact that limits standard N_2 isotherms as a suitable technique for textural analysis of some complex porous systems.[3] By contrast, water molecules (at 25 ºC) reached most of the Stöber microporosity, although aspects concerning the adsorption kinetic restrictions and the unexpected hysteretic behavior remained unanswered. Stöber silica spheres are the most-widely employed monodisperse colloidal beads[3] in material science,[4,5] optics,[6] medicine,[7] etc. Therefore, their adsorption performance –still poorly understood[8,9]– is crucial in many applications, such as catalysis,[10] drug delivery,[11] photonics,[12] or sensing,[13] especially in humid environments.

Here we present a simple procedure to study water adsorption in Stöber spheres by isothermal measurements at different temperatures, applying the Dubinin-Radushkevich (DR) equation for

detailed analysis of both filling and emptying of the Stöber microporosity. We further exploit the DR equation to discern the transition from the micropore filling to the multilayer formation on the outer surface. On the one hand, while it is expected that multilayer adsorption on external surfaces follows filling of the accessible microporosity, both processes are seldom investigated simultaneously. On the other hand, an unexpected interplay between the micropore filling and the subsequent multilayer formation is found and two types of hystereses are observed and discussed. The original methodology followed can be applied to investigate the performance of other porous systems and adsorbates, especially when limited pore accessibility is an issue.

METHODS

Materials and Method. 300-nm Stöber silica monodisperse spheres (Microparticles GmbH) were used in this work. These spheres possess a significant volume of narrow microporosity −as recently proven by CO_2 adsorption isotherms− and no mesoporosity –via N_2 adsorption/desorption isotherms (see analysis of sample SFB-300 in Ref. 2). This choice avoids any influence of the mesopores in the adsorption performance and the associated hysteresis. The narrow microporosity and its intricate morphology, suggested by previous work,[2,9,14,15] make expectable a kinetically restricted accessibility to adsorbates like water, even at ambient temperatures. With this premise, we aim to examine the water adsorption behavior in Stöber microporosity and associated kinetic restrictions. As a straightforward approach, water isotherms at different operational temperature (T) are performed on solid sphere packings of ~ 100 mg. The temperature dependence of the adsorption performance –especially, its reversibility– will provide insights into the processes implicated. Water isotherms were performed in a home-built manometric vapor adsorption system designed and constructed by the LMA (Laboratorio de

Materiales Avanzados) group and now commercialized by Quantachrome as VStar. Prior to each adsorption measurement, the sample was outgassed under ultra-high vacuum conditions at 120 ºC for 12 h. The operational temperatures during adsorption/desorption were T = 10, 25, 40 and 60 ºC. The temperature range was limited by the circulating refrigeration system of the equipment. The water relative pressure p/p_0 was limited to a maximum value $(p/p_0)_{max}$ of 0.9 to prevent capillary condensation in the macroscopic (50-100 nm) interparticle voids between spheres[16] that could interfere with the analysis of the pure ad/desorption processes.

Isotherm Analysis: DR Representation. BET (Brunauer–Emmett–Teller) equation is applied to the adsorption data (up to p/p_0 = 0.15 for the specific case of water adsorption) to determine the apparent surface area (S_{BET}). However, this standard textural characterization only provides indirect insight into microporous features by comparing S_{BET} with the external surface area (S_{ext}) of our Stöber spheres. (The external surface area of a sphere of diameter D and bulk density ρ is calculated by $S_{ext} = 6/(\rho D)$; $\rho \approx 1.83$ g/cm^3 is taken, as obtained by considering an empty volume of 0.1 cm^3/g inside the sphere with amorphous silica density of 2.24 g/cm^3). The DR equation offers a useful −but scarcely exploited− data representation that enables direct inspection of the micropores filling. It is widely accepted in the literature[17,18] that, when the filling of the micropores is *unrestricted*, the adsorption capacity V (the volume of water adsorbed as a liquid) follows the so-called DR equation:[19]

$$\log V = \log V_{micro} - A \log^2\left(\frac{p_0}{p}\right). \qquad (1)$$

This DR representation of the adsorption data, that is, log V vs. $\log^2(p_0/p)$, describes a straight line, which depends on the accessible micropore volume V_{micro}, determined from the y-intercept, and the slope A, associated to the isosteric heat of adsorption at fractional filling of 1/e (E_{ads})[18] by:

$$A = \left(\frac{RT}{E_{ads}}\right)^2 \qquad (2)$$

Although the semi-empirical basis of DR equation may be disputable, involving issues under debate (pressure range of application, compliance with the Henry law at low relative pressures, derivation of heat of adsorption, etc.), it provides a useful framework to quantify the filling of microporosity and the presence of restrictions.[20,21] Specifically, any deviation from linearity of the DR plot means that Eq. (1) is not fulfilled, giving information about processes concurring with the micropore filling. A sublinear region indicates restricted filling of the microporosity; a superlinear region denotes an "adsorption excess" due to additional contributions, typically assigned to adsorption mechanisms beyond the micropore filling, such as condensation in mesoporosity or multilayer formation on outer surfaces.

In this work, we employ the DR representation to analyze in detail the access to the microporosity and the volume filled. The operational temperature T is the varying experimental parameter, which, among the kinetic implications in the filling process, intrinsically affects the slope A through Eq. (2); for illustrative purpose, we show the evolution of an isotherm as a function of T for ideal microporosity filling (see Supporting Information). Unlike the common procedure, we extent the DR analysis to desorption data to examine the micropore emptying process. Thereby, by analogy, the slope A may be associated to the isosteric heat of desorption at fractional filling of 1/e (E_{des}); moreover, symmetrically to adsorption, a restricted evacuation of the microporosity, as it implies limited diminution of V along the desorption branch, leads to superlinearity in the DR plot. Finally, we use the DR equation to generate the adsorption isotherm associated to the ideal micropore filling (see Supporting Information) and analyze the excess due to multilayer formation.

RESULTS AND DISCUSSION

Temperature-dependent Water Isotherm. Figure 1 shows the water isotherms performed at each *T*. The adsorption branches (solid symbols), which reflect the metastable state of adsorption, exhibited a similar shape for all temperatures, with an initial concave rise up to a significant water adsorption capacity, and followed by a continuous growth and an additional increase at higher relative pressures. This shape must be considered as a combination of types I and II, according to IUPAC nomenclature.[22] The type I contribution, at low-mid relative pressures, corresponds to the filling of a considerable microporous volume, where the concave shape reflected the hydrophilicity of the Stöber silica micropores. The type II part is due to the adsorption of water multilayers on the spheres outer surface, which became appreciable at mid-high pressures. The comparison of the adsorption branches revealed subtle but clear differences with temperature (Figure 2a). On the one hand, the adsorption in the low-pressure region was clearly constrained at the lowest *T*, although the branches basically matched at mid-relative pressures. On the other hand, the adsorption growth for higher pressures scaled up with *T*. Regarding the desorption branches, which are close to thermodynamic equilibrium conditions, the temperature dependence was more perceptible (empty symbols in Figure 1). At 10 ºC, water desorption exhibited a marked hysteresis in the high-pressure region (type H4), approached the adsorption branch in the mid pressure region and underwent a second, more noticeable delay at low pressures. By increasing *T*, both high and low pressure hystereses decreased progressively, until almost vanishing at 60 ºC. The temperature-dependent nature of both high and low pressure hystereses is best perceived by direct comparison for all measurements (Figure 2b). The desorption branches, although starting from different points, converged to each other until

merging at $p/p_0 \sim 0.57$ (solid lines in Figure 2b). This point delimited a boundary between both high- and low-pressure hystereses, which appeared to be independent of each other. In fact, the hysteresis at low pressures was reproduced when maintaining $(p/p_0)_{max}$ as low as 0.3.

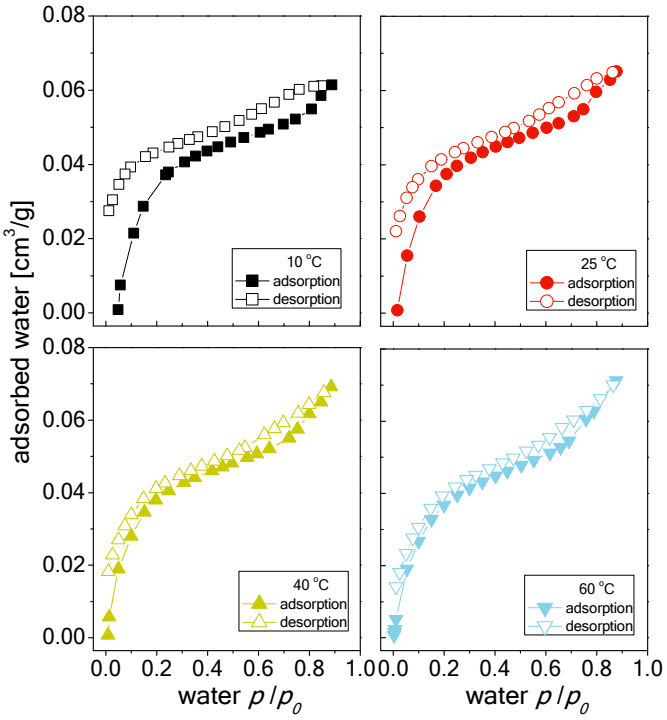

Figure 1. Water adsorption/desorption isotherms performed in 300-nm Stöber spheres up to p/p_0 = 0.89 at different temperatures (10, 25, 40 and 60 ºC). Solid and open symbols are the adsorption and desorption branches, respectively. The adsorbed amount V is expressed as cm^3 of liquid water per g of sample.

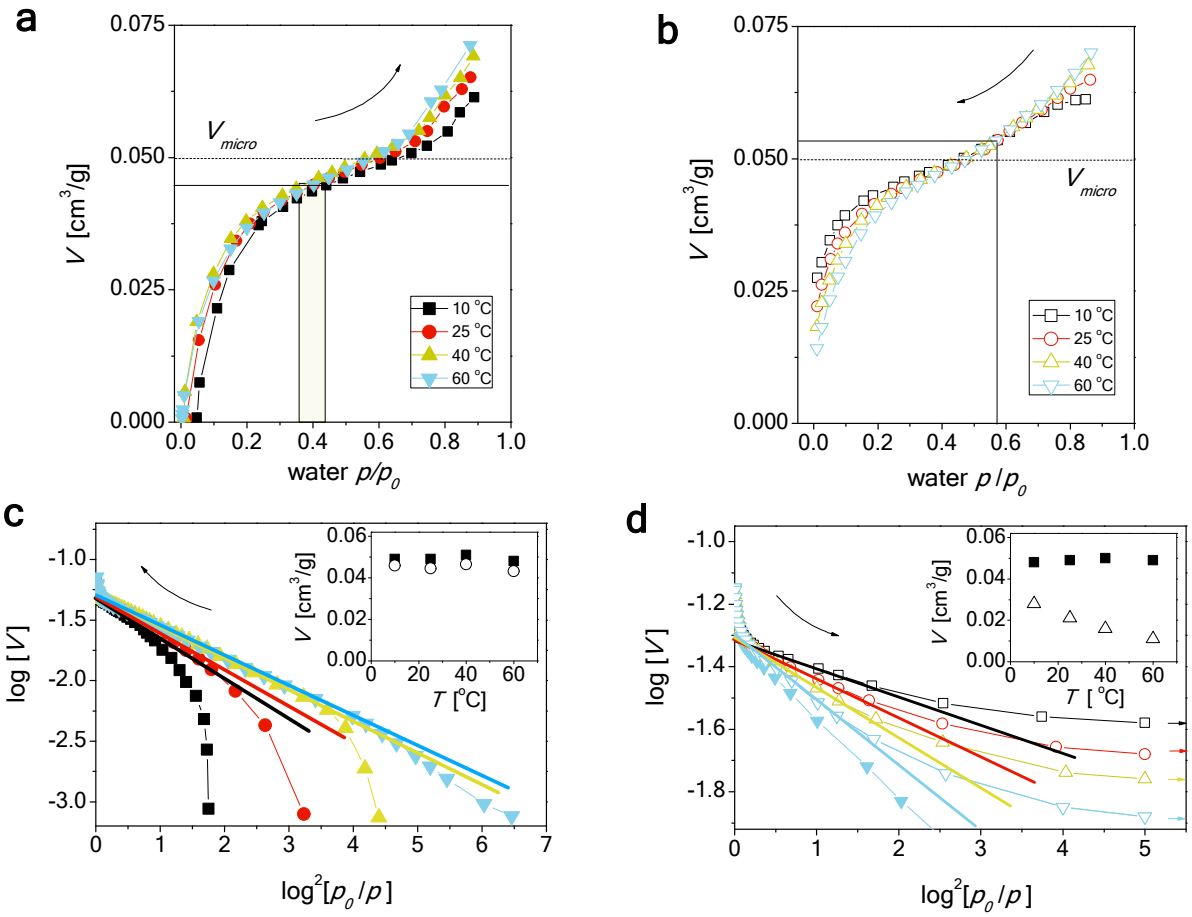

Figure 2. Top: comparison between water adsorption (a) and desorption (b) branches at different temperatures (same data and color code as in Figure 1). Bottom: associated DR plots of adsorption (c) and desorption (d) data (symbols) and corresponding linear regressions (see text). Solid cyan symbols in (d) are adsorption data at 60 ºC for comparison. Insets in (c) and (d) show the relevant volumes obtained from the DR analysis: V_{micro} from linear regressions (solid squares), volume delimiting the end of linearity (open circles in (c)) and V_{res} remaining after desorption (horizontal arrows and open triangles in (d)). Curved arrows indicate the direction of change of p/p_0.

The behavior of desorption manifests the degree of reversibility of the adsorption processes involved,[23] and often reveals their nature. In particular, the occurrence of hysteresis is surprising in these purely microporous Stöber spheres, since no capillary condensation is present. Note that the isotherms were fully reproducible after many cycles, discarding phenomena like silica rehydroxylation.[24,25] Rather, the two distinct hystereses (which are here referred to as low- and high-pressure hystereses) evidenced two well-distinguished delay mechanisms at low and high relative pressures, respectively. We next examine each low- and high-pressure region separately, using the DR representation as a decisive analysis tool. Specifically, the temperature dependencies will provide insight into the corresponding adsorption and desorption mechanisms involved in each region. In addition, we will focus into the transition between both regions, revealing a complex crossover from micropore filling to multilayer formation in these spheres.

Low-Pressure Region: Water Access to Microporosity. BET surface areas obtained from the adsorption branches were around 135 m^2/g in all cases –only slightly smaller for T = 10 ºC (Table 1). Such values, which largely surpassed the outer sphere surface area (S_{ext} = 11 m^2/g), unambiguously attest that the inner volume of the Stöber spheres is substantially microporous and accessible to water molecules. The small kinetic diameter of H_2O (0.265 nm), together with the hydrophilicity of the pore silica walls,[26,27] clearly allowed for significant filling of the microporosity. However, its narrowness (micropore size of 0.3–0.6 nm, as determined by CO_2 adsorption[2]) and tortuosity constitute characteristics to expect *a priori* some access restrictions. Indeed, the temperature-dependent limitation in the adsorption observed in the low pressure region (Figure 2a) points to kinetic constrains, principally at 10 ºC: the lower T (i.e. the lower the kinetic energy of the water molecules), the more limited the adsorption increment.

Table 1. Relevant Parameters obtained from BET and DR Analyses for each Isotherm Temperature

T (ºC)	S_{BET} (m^2/g) [a]	V_{micro} (cm^3/g) [b]	V_{res} (cm^3/g) [c]	E_{ads} (kJ/mol) [b]	E_{des} (kJ/mol) [b]
10	111	0.049	0.028	4.06	8.10
25	136	0.049	0.021	4.90	7.48
40	133	0.051	0.016	5.08	6.42
60	136	0.048	0.011	5.58	6.06

[a] Apparent BET surface area (cross-sectional area for water, 0.106 nm^2). [b] Micropore volume and energies E_{ads} and E_{des} as obtained from DR linear regressions (Eqs. (1) and (2)). [c] Residual volume remaining after desorption.

A convenient data representation to examine the micropore filling –and the occurrence of any restrictions– is given by the DR equation (see next Sections), although it has barely been employed for direct adsorption analysis in microporous systems.[20,21] The DR plot of our adsorption data (Figure 2c, symbols) showed an obvious sublinear behavior at 10 ºC at low relative pressures (high $\log^2(p_0/p)$ values) but gradually mitigated with increasing T, until nearly vanishing at 60 ºC. This pronounced sublinearity and the strong temperature dependence straightforwardly proves a highly restricted accessibility to the microporosity that fundamentally depended on the kinetic energy of the molecules. Hence, the micropore filling was nearly unrestricted only above 40 ºC, and the DR data behaved linearly already at $\log^2(p_0/p) \sim 4$ (relative pressure as low as 0.01). For lower temperatures, the linear region was only achieved at a higher vapor pressure, e.g. at 0.23 for 10 ºC ($\log^2(p_0/p) \sim 0.4$, Figure 2c). The data regression in the linear ranges (straight color lines in Figure 2c) allowed direct quantification of the filled microporosity. The y-intercepts basically coincided for all temperatures, yielding from Eq. (1) a very similar micropore volume $V_{micro} \sim 0.050$ cm^3/g (inset in Figure 2c and Table 1). Thus, regardless of the temperature, the increasing vapor pressure progressively endowed the molecules with sufficient energy to enter the Stöber microporosity, so that they eventually filled the same microporous volume. As a result, despite the temperature-dependent kinetic

restrictions, all adsorption branches matched in a narrow range centered at $p/p_0 \sim 0.4$ (solid lines in Figure 2a).

The emptying of the microporosity exhibited even larger difficulties, as evidenced by the pronounced low-pressure hysteresis (Figure 2b). In analogy to the adsorption analysis, the DR representation of the desorption data (Figure 2d) allows deeper examination. All desorption branches exhibited a limited, but relatively broad, linear region at medium $\log^2(p_0/p)$ values, so that the corresponding linear regressions (straight color lines) determined the micropore volume being evacuated. Again, all y-intercepts approximately converged to a single value, which, consistently, corresponded to the same micropore volume V_{micro} calculated above (inset in Figure 2d). At lower relative pressures (larger $\log^2(p_0/p)$ values), the desorption data in the DR plot became superlinear (Figure 2d), meaning an increasing hindrance to proceed with the micropores emptying. Towards vanishing relative pressures, the evacuated amount tended to an asymptotic value, i.e. a fraction of the micropore volume remained permanently filled. This *residual* volume (V_{res}) of non-desorbed water clearly diminished with increasing T (inset in Figure 2d and Table 1) and serves as a quantification of the inhibited micropore evacuation at each temperature.

The adsorption/desorption behavior in the low- and mid- pressure range demonstrates the water restrictions to access and leave the microporous network of Stöber silica spheres. In particular, the deviation at low pressures in the corresponding DR representation from the linear (ideal) behavior was largely alleviated at increasing temperatures, a fact that evidences the kinetic nature of such limitations. Moreover, no matter the temperature, the water molecules finally overcame the kinetic constraints and the DR plot exhibited a linear region, allowing the calculation of the corresponding heats associated to the filling and emptying of the microporosity using Eq. (2) (Table 1). Figure 3 shows that E_{ads} clearly increased with increasing T, while E_{des}

decreased, so that $E_{des} > E_{ads}$ and both converged to a single value (~ 6 kJ/mol) at high T. However, given the nature of the silica-water interaction (based on hydrogen bond forces[26]) in our system, these heats should barely vary in the narrow temperature span measured (the expected thermodynamic tendency −with constant isosteric heat of adsorption− of the DR slopes is shown in Appendix).

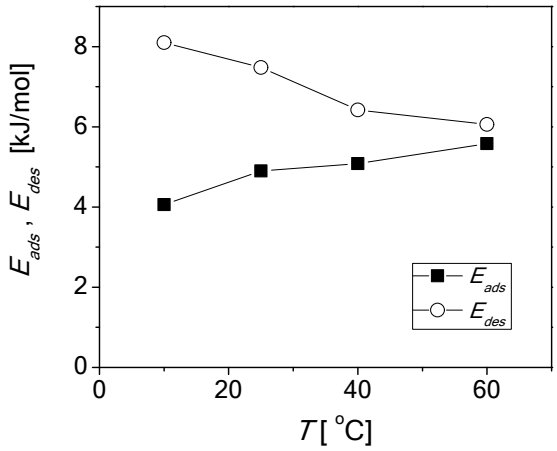

Figure 3. Temperature dependence of the isosteric heats of adsorption and desorption, obtained from DR analysis.

Hence, the variation of E_{ads} and E_{des} with T reflect the occurrence of kinetic restrictions, even in the DR linear regions, to fill and empty the microporosity in our system. Indeed, the micropore filling was strongly restricted in the low-pressure region but exhibited a linear region in the DR plot by increasing the relative pressure, as it allowed better diffusion of the water vapor molecules throughout the microporosity and improved the adsorption rate. However, the fact that the resulting E_{ads} still increased with the adsorption temperature indicates that the diffusion of the strongly interacting water molecules remained partially limited, the more the lower T, so that the DR slope was steeper (apparent E_{ads} was lower) than expected. On the

opposite, hindered diffusion of water molecules out of the micropores during emptying, even in the linear region of the DR desorption data, led to a slope flatter (apparent E_{des} higher) than expected, the more the lower T. By increasing the temperature, the water ability to enter and leave the micropores improved, and both filling and emptying approached the ideal, fully reversible behavior (see both adsorption and desorption data at 60 ºC in Figure 2d). Following this rationale, the behavior shown in Figure 3 is fully coherent, and both E_{ads} and E_{ads} converged to a single value, which may be associated to the actual (for unrestricted conditions), characteristic energy of water in the Stöber microporosity. Consistently, this convergence value is very close to E_{ads} = 6.7 kJ/mol, which is obtained for Stöber micropore filling by a molecule with no access restrictions such as CO_2. The latter value is calculated from the DR plot for CO_2 adsorption data recently measured in Ref. 2, which was perfectly linear over the whole pressure range measured (note that the adsorption energies of water and CO_2, although not identical, are expected to be similar, a fact that justifies this comparison).

According to this, the linearity in the DR representation (Figures 2c, d) corresponds to a pressure region, in which the diffusion of the water molecules within the Stöber microporosity reached its maximum value (for a given temperature), but being still limited by the system constraints. The DR analysis is still valid by interpreting properly the slope, which provides an *apparent* value of E_{ads} that effectively describes the actual micropore affinity to water under the kinetic restrictions present at the experimental conditions. The micropore volumes obtained from the DR linear regressions are also correct, as they consistently coincided, for both adsorption and desorption data and regardless of the temperature, to a single value (0.05 cm^3/g). It is worth noting that this volume is considerably smaller than the total microporous volume probed by CO_2 (0.08 cm^3/g),[2] despite the smaller kinetic diameter of water (0.26 nm vs. 0.33 nm of CO_2).

(Hereby, and for sake of comparison, the same volume for both gases in liquid state was assumed, using the Gurvitch rule[28]). Hence, a fraction of the microporous structure (ca. one-third of its volume) is inaccessible to water, even at the highest temperature measured, and thus not attributable to kinetic reasons. Thus, the specific water-silica interaction appears as the decisive factor explaining the restricted accessibility to the Stöber microporosity. The strong water affinity of the silanols in the micropore walls allows efficient adsorption of the water molecules that are able to reach the inner volume, but it also probably leads to cloaking of narrow micropores, hindering the filling of the total microporous structure (as the non-interacting CO_2 molecules do). In addition, the strong interaction with the pore walls seems to prevail and limit the diffusion of the water vapor molecules within the microporosity, even with high kinetic energy supplied by either increased temperature or pressure, leading to the prominent low-pressure hysteresis observed. Future studies involving, particularly direct kinetic measurements, should lead to a more accurate addressing of these aspects.

Transition to Water Multilayer Adsorption. At mid-high pressures, the adsorption isotherms continued growing, instead of reaching a maximum value at micropore saturation. Such deviation of the type I shape usually signalizes the beginning of adsorption beyond the micropore filling. Given the absence of mesoporosity in the tested spheres,[2] this behavior would denote the formation of water mono- and multilayers adsorbed on the sphere outer surfaces. However, the isotherm shape is too ambiguous to estate the exact point, at which this transition occurs; again, the DR analysis is suitable, as it determines this point by the change from linear to superlinear behavior in the DR adsorption representation. Figure 4a shows that the linear regimes ended at different pressures (the lower, the higher *T*) but at the same adsorbed volume (~ 0.045 cm^3/g) for all temperatures (see also inset in Figure 2c). This volume is somewhat smaller than

V_{micro}, a fact that is implicit in the formalism of Dubinin (see Supporting Information). According to this, the formation of multilayer necessarily begins before the complete filling of the microporosity, which complicates identifying the transition between both contributions. This identification actually concerns the definition of a type II isotherm in the case of a microporous system, that is, when the adsorption data departs from the pure contribution due to the microporosity filling. This may be solved by comparing the experimental isotherm with a hypothetical one that would correspond to the micropore filling contribution solely. The latter can be readily obtained from the linear regressions of the DR adsorption data (Figure 4a) by simple conversion to the usual V - p/p_0 representation (see Supporting Information). These generated adsorption data, which are pure type I isotherms (Figure 4b, solid lines –for clarity, only two temperatures are shown), allow direct visualization of the deviation of the experimental isotherms (symbols). Such deviation quantifies the 'excess' of adsorbed water compared to simple micropore filling (Figure 4c), and it would correspond to the pure type II isotherm due to multilayer formation. Remarkably however, the measured excess exhibited an inflection point at which the slope of the adsorption branch increased, and the isotherm kept growing linearly (dashed straights and regions I-II in Figures 4b,c). This behavior suggests the occurrence of two distinct phenomena contributing to adsorption beyond the simple filling of the Stöber microporosity.

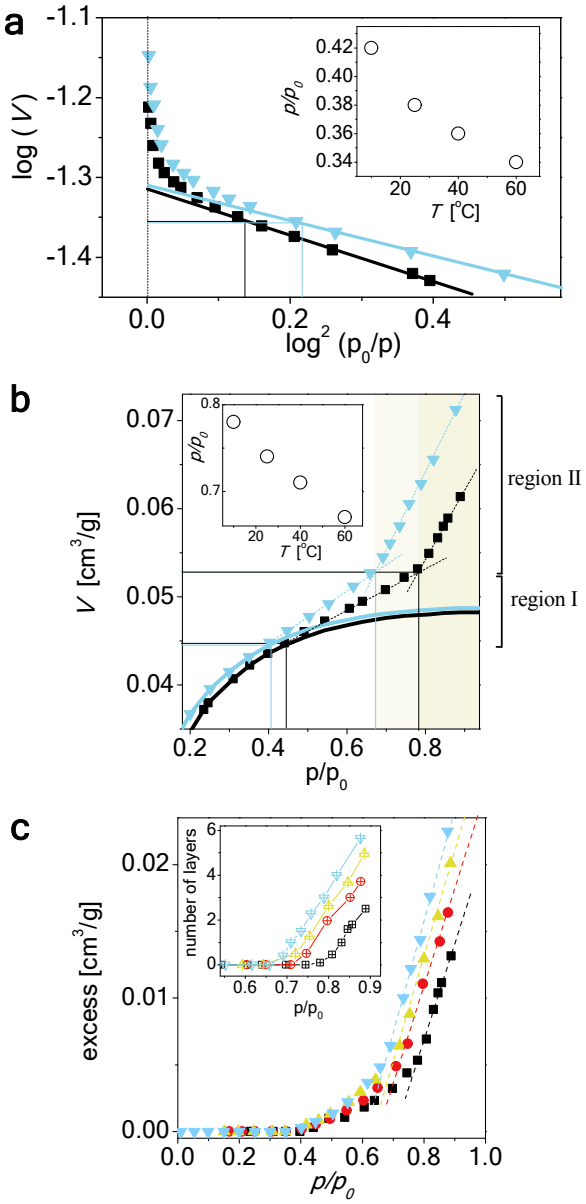

Figure 4. (a) Analysis of the DR adsorption data for determination of the relative pressure (inset) and volume delimiting the end of linearity at each temperature; V is expressed in cm^3/g. (b) Comparison between experimental adsorption data (symbols) and generated data for simple micropore filling (solid curves). Regions I-II (see text) are indicated, and the delimiting relative pressure, as function of the temperature, is shown in the inset. (c) Excess of adsorbed water and number of multilayers (inset). For clarity, the analysis in (a) and (b) is shown only for T = 10 and 60 ºC. Dashed straight lines in (b) and (c) are guide-to-the-eye. Same color code as in Figure 1.

We may assume that the latter increase (region II) is due to water multilayers, since they are expected to progress with increasing pressure in a continuous fashion (until the beginning of capillary condensation in the interparticle macro-porosity, not reached in our experiment). We thus hypothesize that the former adsorption excess (region I) is related to the microporosity itself. Indeed, prior experiments of diverse nature have suggested the occurrence of swelling of Stöber spheres[29,30] (or lattice expansion in colloidal crystals fabricated with them[6,31]) upon water adsorption, which would be ascribed to dilatancy of the microporous structure during its filling.[32] Accordingly, the increased microporous volume allowed additional filling, being responsible for the excess in region I. The limits of this region exhibited a modest but clear downshift with increasing temperature (insets in Figures 4a,b). Nevertheless, the volumes adsorbed at both limits were almost identical: ca. 0.045 and 0.053 cm^3/g, respectively (horizontal lines in Figures 4a, b). Such behavior suggests that the Stöber silica swelling is, on the one hand, was promoted to lower relative pressures with increasing T, which is consistent with easier (less restricted) micropore filling. (Note that any heat-induced dilatancy increment would be negligible in the small temperature span of our experiment). On the other hand, the swelling –or, at least, its noticeable effect on the isotherm– seems to be triggered after filling a certain volume of microporosity and progressed until reaching the same expansion degree, regardless of any temperature-dependent circumstances. The micropore volume after swelling (0.053 cm^3/g), compared to $V_{micro} \sim 0.050$ cm^3/g, corresponded to an increment of 2% of the sphere volume (0.07% of the sphere diameter).

When the filling of the swelled micropore volume also saturated, multilayer adsorption became significant, which is appreciated as a slope change in the adsorption branch (region II in Figure 4b). Subtracting the swelling contribution (region I) to the adsorption excess, we obtain the net

contribution to the isotherm of the water multilayers, and their evolution with increasing relative pressure. By assuming that the multilayer adsorption on the hydrophilic Stöber silica basically proceeds homogeneously (by contrast with cluster-like formation on rather hydrophobic silica surfaces),[26,33] we can calculate the number of layers adsorbed by considering 0.003 g/cm^3 per monolayer, as obtained from the sphere S_{ext} and the water molecular cross-section (0.106 nm^{-2}). (Note that, if no sphere swelling is considered, the estimated number of layers would only increase in about 1 layer). The resulting multilayer behavior (inset in Figure 4c) offers two main relevant features. The first one is the existence of an onset for multilayer adsorption, a fact that contradicts the usual adsorption behavior observed on surfaces, in which the buildup of molecular layers of adsorbate is continuous from the low-pressure region.[34,35,36] That is, the porous nature of the Stöber silica prevented the adsorption of water molecules on the external spheres surface until the microporosity was completely filled. This implies a sequential adsorption process, i.e. first, narrower pores are filled, and subsequent adsorption follows on wider pores or open surfaces. The characteristics of our system allowed distinguishing this behavior, which is typically assumed in multi-porous systems but has rarely been measured directly. Quantitatively, the number of adsorbed layers (at p/p_0 = 0.89, from 3 to 6 layers for 10 to 60 ºC, respectively) agrees well with the values reported in the literature for water adsorption on different silica surfaces.[37,38,39,40,41] That is, the multilayer formation, after a delayed start, rapidly progressed in a linear fashion (inset in Figure 4c) –instead of the convex growth typically observed in nonporous materials[35,36,39]– to finally achieve a similar adsorbed amount at high pressures.

The second relevant feature is that the water multilayer formation was apparently favored at higher T: the onset shifted to lower relative pressure and the number of adsorbed layers increased

(Figure 4c, inset). This discovery is surprising, as it is contrary to the expected behavior, according to which the adsorption of vapor molecules with lower kinetic energy (lower temperature) is improved. The explanation would rather rely on the different evolution of the microporosity filling, which delays the onset of the multilayer adsorption, as discussed above. In such scenario, the restricted access to the sphere microporosity is relieved with increasing T –as shown in Section 3.2– and the adsorption on the outer surface started sooner (inset in Figure 4c). This way, the dissimilar accessibility to the narrow Stöber porosity, leading to a different progression in the micropore filling, induced a significant, temperature-dependent alteration in the multilayer formation. Interestingly, the evolution after the onset was basically temperature-independent, as the multilayers grew with the same slope for all T.

High-Pressure Hysteresis. A pronounced hysteresis at high relative pressure was obtained in the Stöber spheres, as the desorption branch clearly deviated in its early stage from the adsorption branch (Figure 1). Remarkably, all desorption branches converged to a single point at $p/p_0 \sim 0.57$ (Figure 5a), which serves as a boundary pressure between the high- and low-pressure hystereses, as pointed above. Interestingly, the adsorbed volume at this point coincides with the 'swelled' microporous volume of 0.053 cm^3/g deduced in the previous Section. In other words, the high-pressure hysteresis finished when all the external (multilayer) water was removed, remaining only the adsorbed amount filling the microporosity. Expectedly, the micropore emptying began only thereafter, when the micropore mouths became in contact with the gas phase. This behavior agrees with recent NMR relaxometry experiments in Stöber spheres[42] and further supports the interpretation that the desorption behavior in the middle low-pressure range, including the occurrence of low-pressure hysteresis, only concerns the emptying of the Stöber microporosity.

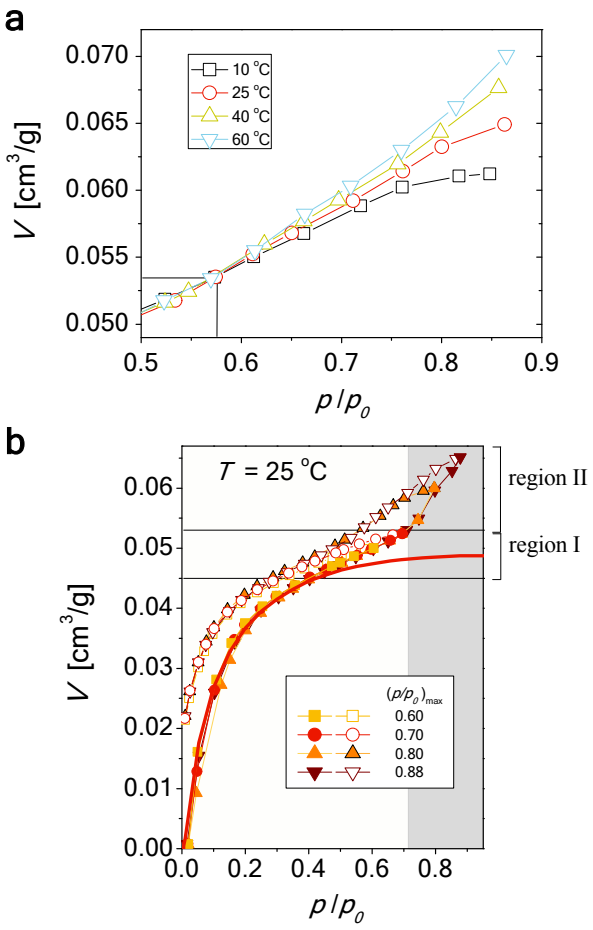

Figure 5. (a) Close-up of the desorption data; a convergence point is indicated. (b) Water adsorption and desorption isotherms performed at different $(p/p_0)_{max}$ and constant T = 25 ºC (symbols). Regions I-II and generated data for simple micropore filling (red line) are indicated as a reference.

In turn, the high-pressure hysteresis logically appears to be related to the evolution of the water multilayers formed on the spheres outer surface. Hence, its occurrence does reflect a delay between multilayer adsorption and desorption, which is uncommon in multilayer adsorption experiments performed on surfaces. The observed temperature dependence, being the hysteresis most prominent at 10 ºC and almost vanishing at 60 ºC (Figure 1), suggests again a kinetic origin. Actually, as inferred from the previous Section, the temperature dependence of the

multilayer adsorption was only apparent, so that the onset of this process was deferred to higher pressures by the restricted micropore filling, the more, the lower *T*. By contrast, the multilayer desorption followed the expected tendency with temperature, i.e. the easier, the higher *T*. In fact, the desorption branch in the high-pressure region was flatter at 10 ºC and steeped with increasing *T* (Figure 5a). As a consequence, we find that the hysteretic behavior of the adsorbed multilayers is indirectly caused by the kinetically limited filling of the microporous volume in the Stöber spheres, which delays the multilayer formation, while the multilayer desorption is unaffected because the microporosity remains filled during this stage. Thus, it takes place a non-trivial interplay between microporosity (which is filled in the low-mid pressure range) and the hysteresis loop in the high-pressure region. At the highest temperature (60 ºC), the restrictions to micropore filling were greatly attenuated and the isotherm approached a reversible behavior, also in the high-pressure region. Consistently to this explanation, we have observed a negligible high-pressure hysteresis in nonporous (achieved by thermal treatment) Stöber spheres, approaching the adsorption/desorption behavior of standard silica surfaces.

Finally, we performed an additional experiment that explicitly demonstrates the gradual suppression of the high-pressure hysteresis by avoiding the formation of the water multilayers. A series of water isotherms at the same temperature (T = 25 ºC) was measured at different $(p/p_0)_{max}$ values. Figure 5b shows that the isotherms presented no high-pressure hysteresis as $(p/p_0)_{max} < 0.75$, which is the pressure at which water multilayers began to form for 25 ºC (Figure 4). By contrast, the isotherms with $(p/p_0)_{max} > 0.75$ exhibited a clear hysteresis loop in the high-pressure range, confirming its direct correlation to the adsorbed multilayers. In all cases, the progress of the desorption branches was identical in the middle low-pressure region, which only concerned

the emptying of the micropores, being thus entirely independent of pre-existing adsorbed multilayers.

CONCLUSIONS

Water adsorption isotherms on microporous Stöber silica spheres were performed at different temperatures, atypically exhibiting two well-distinguished, temperature-dependent hystereses. At low relative pressures, the Dubinin-Radushkevich representation (applied to both adsorption and desorption data) evidenced that water molecules underwent significant kinetic restrictions to fill and empty the Stöber microporosity, leading to a pronounced low-pressure hysteresis. The associated isosteric heats, provided by the DR analysis, reflected the progressive attenuation of the kinetic constraints for higher temperatures, although some fraction of the micropore volume remained inaccessible, likely due to the strong interaction silica-water. The adsorption evolution with increasing pressure was analyzed by deconvoluting the experimental data into a type-I (due to micropore filling, using DR equation) and type-II (due to the subsequent multilayer formation) isotherms. An unexpected adsorption contribution was identified and attributed to swelling of the Stöber spheres, which allowed additional micropore filling. The number of water multilayers adsorbed on the spheres outer surface was estimated, finding an anomalous, temperature-dependent delay to higher pressures, ascribed to the restrictions in the prior micropore filling. As a result, a high-pressure hysteresis was obtained, which directly correlated to the formation of water multilayers. A fully reversible adsorption behavior (non-hysteretic isotherms) was approached when the constraints to access the Stöber microporosity were sufficiently relieved, as in the case of increased operational temperature.

ASSOCIATED CONTENT

Supporting Information Available: Ideal micropore filling: adsorption isotherms and Dubinin-Radushkevich representation and Adsorption beyond micropore filling: Dubinin-Radushkevich representation. This material is available free of charge via the Internet at http://pubs.acs.org.

AUTHOR INFORMATION

Corresponding Author

F. Gallego-Gómez; Email: francisco.gallego@icmm.csic.es

J. Silvestre-Albero: joaquin.silvestre@ua.es

Author Contributions

The manuscript was written through contributions of all authors. All authors have given approval to the final version of the manuscript.

ACKNOWLEDGMENT

This work was funded by Spanish MINECO projects MAT2014-58731-JIN and MAT2016-80285-p, and Spanish MCIU project RTI2018-093921-B-C41.

REFERENCES

[1] Rios, R. V. R. A.; Silvestre-Albero, J.; Sepúlveda-Escribano, A.; Molina-Sabio, M.; Rodríguez-Reinoso, F. Kinetic restrictions in the characterization of narrow microporosity in carbon materials. *J. Phys. Chem. C* **2007**, *111*, 3803−3805.

[2] Farrando-Pérez, J.; López, C.; Silvestre-Albero, J.; Gallego-Gómez, F. Direct Measurement of Microporosity and Molecular Accessibility in Stöber Spheres by Adsorption Isotherms. *J. Phys. Chem. C* **2018**, *122*, 22008−22017.

[3] Stöber, W.; Fink, A.; Bohn, E. Controlled Growth of Monodisperse Silica Spheres in the Micron Size Range. *J. Colloid Interface Sci.* **1968**, *26*, 62-69.

[4] Quan, W.; Ramsey, C.; Baran; Q. Thermal pretreatment of silica composite filler materials. *J Thermal Analysis Calorimetry* **2009**, *99*(1), 237-243.

[5] Fan, L.; Josephson, D. P.; Stein, A. Colloidal assembly: the road from particles to colloidal molecules and crystals. *Angew. Chem. Intern. Ed.* **2011**, *50*, 360-388.

[6] Gallego-Gómez, F.; Blanco, A.; López, C. Exploration and Exploitation of Water in Colloidal Crystals. *Adv. Mater.* **2015**, *27*, 2686–2714.

[7] Meddahi-Pell, A.; Legrand, A.; Marcellan, A.; Louedec, L.; Letourneur, D.; Leibler, L. Organ Repair, Hemostasis, and In Vivo Bonding of Medical Devices by Aqueous Solutions of Nanoparticles. *Angew. Chem. Int. Ed.* **2014**, *53*, 6369 –6373.

[8] Gallego-Gómez, F.; Morales-Flórez, V.; Morales, M.; Blanco, A.; López, C. Colloidal crystals and water: Perspectives on liquid–solid nanoscale phenomena in wet particulate media. *Adv. Colloid Interface Sci.* **2016**, *234*, 142-160.

[9] Li, S.; Wan, Q.; Qin, Z.; Fu, Y.; Gu, Y. Understanding Stöber silica's pore characteristics measured by gas adsorption. *Langmuir* **2015**, *31*, 824–832.

[10] Yang, M.; Wu, H.; Wu, H.; Huang, C.; Weng, W.; Chen, M.; Wan, H. Preparation and characterization of a highly dispersed and stable Ni catalyst with a microporous nanosilica support. *RSC Adv.* **2016**, *6*(84), 81237-81244.

[11] Xu, Z.; Liu, S.; Kang, Y.; Wang, M. Glutathione-and pH-responsive nonporous silica prodrug nanoparticles for controlled release and cancer therapy. *Nanoscale* **2015**, *7*(13), 5859-5868.

[12] Gallego-Gómez, F.; Blanco, A.; López, C. Photoinduced local heating in silica photonic crystals for fast and reversible switching. *Adv. Mater.* **2012**, *24*, 6204–6209.

[13] Gallego-Gómez, F.; Morales, M.; Blanco, A.; López, C. Bare Silica Opals for Real-Time Humidity Sensing. *Adv. Mater. Technol.* **2019**, *4*, 1800493.

[14] Labrosse, A.; Burneau, A. Characterization of Porosity of Ammonia Catalysed Alkoxysilane Silica. *J. Non-Cryst. Solids* **1997**, *221*, 107−124.

[15] Szekeres, M.; Toth, J.; Dekany, I. Specific Surface Area of Stober Silica Determined by Various Experimental Methods. *Langmuir* **2002**, *18* (7), 2678−2685.

[16] Gallego-Gómez, F.; Morales, M.; Blanco, A.; López, C. Tunable Visual Detection of Dew by Bare Artificial Opals. *Adv. Funct. Mater.* **2018**, *28*(21), 1800591.

[17] Gil, A.; Grange, P. Application of the Dubinin-Radushkevich and Dubinin-Astakhov equations in the characterization of microporous solids. *Colloids Surf. A: Phys. Eng. Aspects* **1996**, *113*(1-2), 39-50.

[18] Kaneko, K.; Murata, K. An analytical method of micropore filling of a supercritical gas. *Adsorption* **1997**, *3*(3), 197-208.

[19] Rouquerol, F.; Rouquerol, J.; Sing, K. Adsorption by powders and porous solids, 2nd Ed., Academic Press, London, 2013.

[20] Kapoor, A.; Ritter, J. A.; Yang, R. T. On the Dubinin-Radushkevich equation for adsorption in microporous solids in the Henry's law region. *Langmuir* **1989**, *5*(4), 1118-1121.

[21] Nguyen, C.; Do, D. D. The Dubinin–Radushkevich equation and the underlying microscopic adsorption description. *Carbon* **2001**, *39*(9), 1327-1336.

[22] Thommes, M.; Kaneko, K.; Neimark, A. V.; Olivier, J. P.; Rodriguez-Reinoso, F.; Rouquerol, J.; Sing, K. S. W. Physisorption of gases, with special reference to the evaluation of surface area and pore size distribution (IUPAC Technical Report). *Pure Appl.Chem.* **2015**, *87*, 1051-1069.

[23] Ravikovitch, P. I.; Domhnaill, S. C. O.; Neimark, A. V.; Schüth, F.; Unger, K. K. Capillary hysteresis in nanopores: Theoretical and experimental studies of nitrogen adsorption on MCM-41. *Langmuir* **1995**, *11*, 4765-4772.

[24] Baker, F. S.; Sing, K. S. Specificity in the adsorption of nitrogen and water on hydroxylated and dehydroxylated silicas. *J. Colloid Interface Sci.* **1976**, *55*(3), 605-613.

[25] Legrand, A. P.; Hommel, H.; Tuel, A.; Vidal, A.; Balard, H.; Papirer, E.; Levitz, P.; Czemichowski, M.; Erre, R.; Van-Damme, H.; et al. Hydroxyls of silica powders. *Adv. Colloid Interface Sci.* **1990**, *33*, 91.

[26] Zhuravlev, L. T. Surface characterization of amorphous silica—a review of work from the former USSR. *Colloids Surf. A* **1993**, *74*(1), 71-90.

[27] Gallego-Gomez, F.; Blanco, A.; Golmayo, D.; Lopez, C. Three regimes of water adsorption in annealed silica opals and optical assessment. *Langmuir* **2011**, *27*, 13992.

[28] Cychosz, K. A.; Guillet-Nicolas, R.; Garcia-Martinez, J.; Thommes, M. Recent advances in the textural characterization of hierarchically structured nanoporous materials. *Chem. Soc. Rev.* **2017**, *46*, 389-414.

[29] de Keizer, A.; van der Ent, E. M.; Koopal, L. K. Surface and volume charge densities of monodisperse porous silicas. *Colloids Surf. A* **1998**, *142*, 303.

[30] Costa, C. A.; Leite, C. A.; Galembeck, F. Size dependence of Stöber silica nanoparticle microchemistry. *J. Phys. Chem. B* **2003**, *107*(20), 4747-4755.

[31] Gallego-Gómez, F.; Blanco, A.; Canalejas-Tejero, V.; Lopez, C. Water-dependent photonic bandgap in silica artificial opals. *Small* **2011**, *7*, 1838-1845.

[32] Gor, G. Y.; Huber, P.; Bernstein, N. Adsorption-induced deformation of nanoporous materials—a review. *Appl. Phys. Rev.* **2017**, *4*(1), 011303.

[33] Blanco, A.; Gallego-Gómez, F.; López, C. Nanoscale Morphology of Water in Silica Colloidal Crystals. *J. Phys. Chem. Lett.* **2013**, *4*, 1136−1142.

[34] Pashley, R. M. Multilayer adsorption of water on silica: An analysis of experimental results. *J. Colloid Interface Sci.* **1980**, *78*(1), 246-248.

[35] Gee, M. L.; Healy, T. W.; White, L. R. Hydrophobicity effects in the condensation of water films on quartz. *J. Colloid Interface Sci.* **1990**, *140*(2), 450-465.

[36] Beaglehole, D.; Christenson, H. K. Vapor adsorption on mica and silicon: entropy effects, layering, and surface forces. *J. Phys. Chem.* **1992**, *96*(8), 3395-3403.

[37] Plooster, M. N.; Gitlin, S. N. Phase transitions in water adsorbed on silica surfaces. *J. Phys. Chem.* **1971**, *75*(21), 3322-3326.

[38] Hagymassy, J., Jr.; Brunauer, S.; Mikhail, R. S. Pore structure analysis by water vapor adsorption: I. t-curves for water vapor. *J. Colloid Interface Sci.* **1969**, *29*(3), 485-491.

[39] Naono, H.; Hakuman, M. Analysis of adsorption isotherms of water vapor for nonporous and porous adsorbents. *J. Colloid Interface Sci.* **1991**, *145*(2), 405-412.

[40] Raoof, A.; Guilbaud, J. P.; Van Damme, H.; Porion, P.; Levitz, P. Analysis of the multilayer thickness relationship for water vapor and nitrogen adsorption. *J. Colloid Interface Sci.* **1998**, *206*(1), 1-9.

[41] Asay, D. B.; Kim, S. H. Evolution of the adsorbed water layer structure on silicon oxide at room temperature. *J. Phys. Chem. B* **2005**, *109*(35), 16760-16763.

[42] Gallego-Gómez, F.; Cadar, C.; Lopez, C.; Ardelean, I. Microporosity Quantification via NMR Relaxometry. *J. Phys. Chem. C* **2019**, *123*(50), 30486-30491.

TOC IMAGE

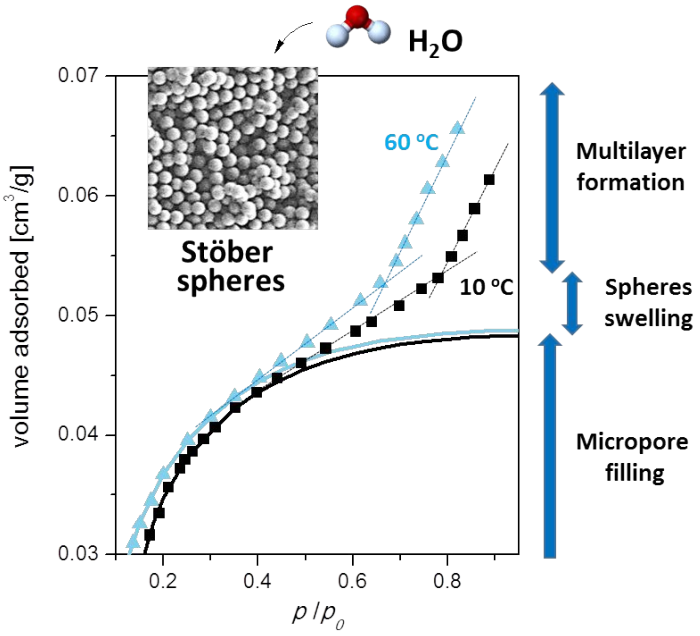
H2O
0.07
0.06
0.05
0.04
0.03
volume adsorbed [cm3/g]
0.2
0.4
0.6
0.8
p / p0
Stöber spheres
60 °C
10 °C
Multilayer formation
Spheres swelling
Micropore filling